PAN
ARCHIVES OF ACOUSTICS
Vol. **44**, No. 3, pp. 585–601 (2019)
DOI: 10.24425/aoa.2019.129273

Estimation of the Azimuth Angle of the Arrival Direction for an Ultrasonic Signal by Using Indirect Determination of the Phase Shift

Bogdan KRECZMER

Department of Cybernetics and Robotics
Faculty of Electronics
Wrocław University of Science and Technology
Janiszewskiego 11/17, 50-372 Wroclaw, Poland; e-mail: bogdan.kreczmer@pwr.edu.pl

(*received October 14, 2018; accepted June 6, 2019*)

The paper presents and discusses a method of azimuth determination of ultrasonic echo arrival in air. The basis of the presented approach is the assumption that the received signal is a narrowband one. In this way, the direction of the signal arrival can be determined based on its phase shift using two receivers. When the distance between the receivers exceeds half of the wavelength of the received signal, a problem of ambiguity in determining the angle of arrival arises. To solve this, a method using multiple pairs of receivers was used. Its robustness and temperature dependence is analysed. The most important advantages of the presented approach are simplified computations and low hardware requirements. Experimental data made it possible to show that for strong echoes, the accuracy is higher than 0.5°. In the case of weak echos, it is reduced to about 2°. Because the method is based on phase shift measurement, the ultrasonic sonar that uses this method can be compact in size. Moreover, owing to the theoretical analysis, certain properties of the mutual location of the receivers were found and formally proved. They are crucial for determining proper receivers' inter-distances.

Keywords: ultrasonic range finder; sonar; direction of arrival.

1. Introduction

Popular ultrasonic range finders are very pure in angular resolution, and can therefore not be effectively used in the navigation of mobile robots. This can be changed by using sonars that are able to determine the distance to an object and the direction of arrival (DOA) of a received echo. In order to replace simple ultrasonic range finders with such sonars, their method of DOA determination should be simple enough to minimize the necessary hardware and software in order to make the sensor compact in size. In (Kreczmer, 2017), an approach that makes it possible to estimate the DOA using the indirect determination of the phase shift is presented. Because it does not rely on a signal amplitude measurement, no sampling is needed and computations are simplified. In this paper, a more detailed analysis and its theoretical justification are presented. The performed tests and experiments showed that the method combined the simplicity of computation and the precision and accuracy of DOA determination. Moreover, it is shown that this approach can be extended in a simple way to the 3-D case in which the distance and azimuth, as well as elevation angles are determined. The remainder of this paper is organized as follows: Sec. 2 gives a brief overview of related studies; Sec. 3 contains the formulation of the analysed problem and a signal model, and also describes the main assumptions of the presented approach; Sec. 4 presents a method of azimuth angle determination of an ultrasonic echo; Sec. 5 discusses the problem of solution ambiguity when the inter-distance between receivers is bigger than half of the wavelength of a received signal; Sec. 6 analyses the influence of measurement errors on the determined value of the azimuth angle of signal arrival; Sec. 7 describes the improvement of the presented approach by introducing more pairs of receivers; Sec. 8 presents the dependence between temperature and the accuracy of measurements and also gives an explanation of the observed phenomena; The next section shows the results of experiments; and finally, in the last regular section, the main conclusions

are summarized. In Appendix, several theorems describing features of the mutual location of the receivers, as well as their proofs, are presented. They are crucial for determining proper receivers' inter-distances. This is important because the presented approach is sensitive to these values.

2. Related work

When a signal source is relatively close to receivers, the problem of DOA determination can be solved by using triangulation methods based on range difference information. The critical point in triangulation methods is the determination of the time of signal flight. To overcome this problem, signal modulation combined with correlation function methods were applied in (Walter, Schweinzer, 2014). Range difference can also be measured by utilizing the signal phase shift (Choi *et al.*, 2014).

The most common approach to DOA determination is based on array signal processing, and is used in many applications of radar, sonar or communication. The well-known method is multiple signal classification (MUSIC) (Schmidt, 1986). There are several variants of this method, e.g. root-MUSIC (Zhang *et al.*, 2017), the total spectral search MUSIC method (Zhou *et al.*, 2013), or the partial spectral search one (Sun *et al.*, 2015). Another well-known approach to DOA determination is the estimation of signal parameters via rotational invariance techniques (ESPRIT) (Roy *et al.*, 1986; Roy, Kailath, 1989). This approach also has a lot of variants and adaptations, e.g. Unitary ESPRIT (Haardt, Nossek, 1995), Conjugate ESPRIT (Tayem, Kwon, 2003). The important advantage of these methods is that they make it possible to determine the DOA of signals emitted by several sources, but they unfortunately require complex computations. Even the improvement of such a method that was presented in (Yang *et al.*, 2018) still contains a lot of float-point operations. In (Clapp, Etienne-Cummings, 2006), a hardware-based approach was presented. A mixed-signal full-custom VLSI chip was designed to receive acoustic signals from an ultrasonic microphone array. It made it possible to extract the input bearing angles of the incoming wave. The processing utilizes simple low-power analog spatiotemporal bandpass filters to extract wavefront velocity across the array, which is translated to the input bearing angle. Spatial filters are also used in (Steckel *et al.*, 2013). The presented method applies an array beamforming technique to the synthesis of 3-D spatial filters. By combining broadband beamforming with a sparse and random array of MEMS microphones, the obtaining of 3-D location measurements in the presence of multiple highly overlapping echoes is permitted. This type of sonar appeared to be very effective and made it possible to implement the system BatSLAM (Steckel, Peremans, 2013) which was able to solve the simultaneous localization and mapping problem (SLAM) (Steckel, Peremans, 2015). MEMS microphones were also used in (Herman *et al.*, 2014) to create a linear array. The DOA was determined by implementing of beamforming algorithms. To measure distance, a correlation function-based method was applied.

In (Im *et al.*, 2013), another approach to processing signals received on an array of microphones was presented. The approach is based on a cumulated signal amplitude in a single period. Because this approach assumes that the maximal amplitude of a signal is the same during a long period of time, it is difficult to meet this assumption in practical implementation.

To obtain a very good accuracy of DOA determination, the discussed approaches involve methods that are relatively computationally expensive. Most of them are able to determine the DOA of signals that come from several sources. The approach presented in this paper is restricted to the problem of DOA determination for an echo coming from a single direction. This is the obvious drawback. However, when an emitted signal is short enough, it can be acceptable for many applications of mobile robot navigation. The important advantages are that the computational burden is reduced and the hardware requirements are very low. Despite this, a very good accuracy of DOA estimation is obtained. In this sense, the presented method can be exploited in order to build an inexpensive sonar that will be a good replacement of traditional ultrasonic range finders.

3. Problem formulation and signal model

The 3-D problem of the localization of an object by using a sonar (see Fig. 1a) consists of finding the distance to the object, as well as finding the

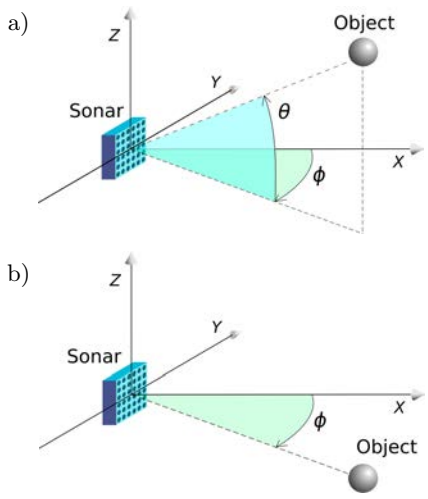

Fig. 1. Sonar application to the localization of the object in: a) 3-D space, b) the horizontal plane.

azimuth and elevation angles i.e. (r, ϕ, θ). The distance is determined by measuring the time-of-flight (TOF). The angles are obtained by estimating the DOA. When the object is located in the horizontal plane (see Fig. 1b) and only such object locations are considered, the only angle of the DOA to determine is the azimuth angle. In this sense, the problem is reduced to a 2-D one (r, ϕ). This paper is focused on a method of determining the azimuth angle of the DOA. To determine TOF, one of the well-known methods can be used. It is worth noting that when the sonar receiver system has axial symmetry, it is simple to extend it to the 3-D case. It is enough to use two such systems which are perpendicular to each other. The angles determined by both systems make it possible to estimate the azimuth and elevation angles. Therefore, it is worth studying features of the 2-D case.

It is assumed that the signal emitted, and then received, is narrowband. This assumption is especially true when piezoelectric transducers are used. In this case, the signal can be modelled by the function

$$S(t) = 1(t-t_0)\left((t-t_0)^{p_1} M_1 e^{-\frac{t-t_0}{\tau_1}} + (t-t_0)^{p_2} M_2 e^{-\frac{t-t_0}{\tau_2}}\right) \cdot A\sin\left(\omega(t-t_0)+\gamma\right) + n(t), \quad (1)$$

where t_0 is the time of signal arrival, M_1 and M_2 determine the signal magnitude, p_1, p_2, τ_1, τ_2, and γ are transducer constants, ω is the angular frequency of the ultrasound and $n(t)$ is the noise of the signal. Figure 2a presents the oscillogram, which shows the signal received by the receiver MA40S4R produced by Murata. The signal was emitted by the transducer BPU-1640T0AH12 produced by Bestar. The gap between the emitter and the receiver was 93 mm. Using Eq. (1), the approximate model of the signal can be obtained for the following parameter values: $M_1 = 3.46 \cdot 10^{-9}$ µs^{-4}, $M_2 = 8.30 \cdot 10^{-6}$ µs^{-2}, $p_1 = 4$, $p_2 = 2$, $\tau_1 = 80$ µs, $\tau_2 = 300$ µs, $A = 723$ mV, $\gamma = 0°$, and $\omega = 2\pi f_s$ where the signal frequency $f_s = 40.91$ kHz. For simplicity, it was assumed that $n(t) \equiv 0$. Figure 2b presents its diagram. The key feature of the observed signal, which is exploited in the proposed approach, is that its frequency is not changed rapidly. In fact, it hardly changes at all. In addition, it is assumed that inter-distances between receivers are small compared to the distance to the object. This justifies the assumption that the acoustic wave reflected by the object, and then registered by sonar receivers, can be treated as a planewave in the vicinity of the receivers.

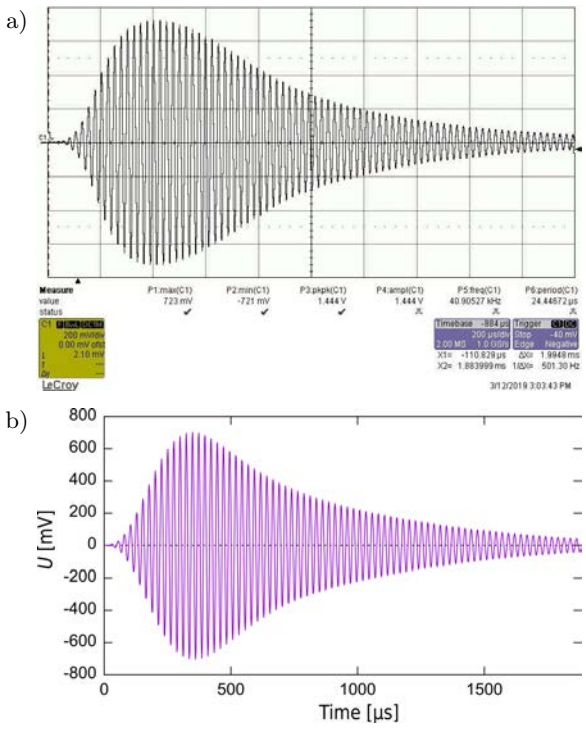

Fig. 2. a) The oscillogram of a signal transmitted by the transducer BPU-1640T0AH12 and received by the receiver MA40S4R; b) the diagram of the signal model.

4. Determination of signal arrival direction

DOA estimation by using phase shift measurements is a well-know approach. It can be applied when a signal has a narrow bandwidth and the distance between receivers is lower than a half wavelength (see Fig. 3). Because of assumptions stated at the end of the previous section, the echo wave is treated as a planewave. This makes it possible to determine the incident angle by using the following simple formula:

$$\phi = \arcsin\frac{s}{b} = \arcsin\frac{v_a \tau}{b}, \quad (2)$$

where s is the distance of a wavefront to the receiver R_1 at the moment when the wavefront reached the receiver R_0 (see Fig. 3), v_a is the speed of the acoustic wave, b is the distance between receivers R_0 and R_1, and τ is the interval time between the moment of wavefront detection by the first receiver and, then, by the second one. In this paper, it is assumed that receivers, as well as a signal source, are located in the same horizontal plane. Therefore, the incident angle of the signal is the azimuth angle Fig. 4.

It is impossible to determine the angle correctly due to the inter-distance b between receivers being bigger than a half of the signal wavelength. In this case, it is

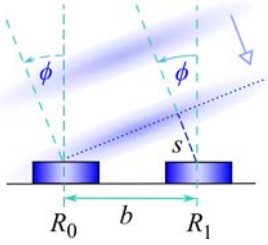

Fig. 3. A wavefront of a planewave propagated towards two receivers.

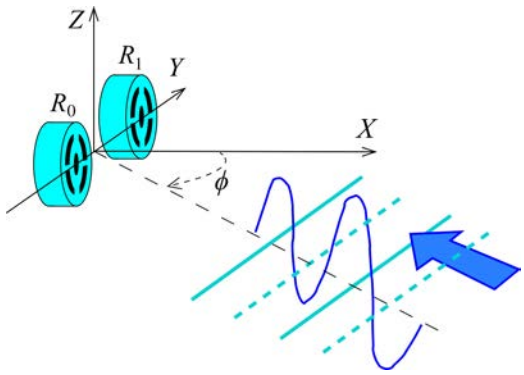

Fig. 4. Location of the receivers in the 3-D coordinate system.

a phase ambiguity of an integer multiple of 2π between the actual and the observed phase shifts due to phase wrapping. It means that it is possible to obtain a few angle values ϕ_i for which integer numbers n_i exist that determine ϕ_i as follows

$$\phi_i = \arcsin \frac{v_a\tau + n_i\lambda}{b}, \tag{3}$$

where λ is the wavelength of the signal. When ϕ is known, the correct value of n can be determined by the formula

$$n = \left\lfloor \frac{b\sin\phi}{\lambda} \right\rfloor \lambda,$$

where $\lfloor . \rfloor$ is the floor function. Using this formula, it allows the interval time τ by ϕ to be expressed as follows

$$\tau(\phi) = \frac{1}{v_a}\left(b\sin\phi - \left\lfloor \frac{b\sin\phi}{\lambda} \right\rfloor \lambda\right). \tag{4}$$

When τ is measured and the correct value of ϕ is unknown, the set of all possible values of n_i that can be used in Eq. (3) can be defined as follows

$$\mathcal{I}_\Phi(\tau, b)_\tau = \left\{ n_i : n_i \in \mathbf{I} \wedge \sin\phi_{\min} \le \frac{v_a\tau + n_i\lambda}{b} \le \sin\phi_{\max} \right\},$$

where $\mathbf{I}$ is the set of integer numbers and $\phi_{\min}$ and $\phi_{\max}$ determine the range $\Phi = [\phi_{\min}, \phi_{\max}] \subseteq (-\frac{\pi}{2}, \frac{\pi}{2})$. This is the range of azimuth angles for which measurements can be performed. The additional subscript τ was used in order to emphasize that this set is determined using a measured value of τ when ϕ is unknown. However, sometimes it will be useful to determine this set for a known ϕ, which is possible because of Eq. (4). In that case, the notation $\mathcal{I}_\Phi(\phi, b)_\phi$ will be applied.

When $b > \frac{\lambda}{2}$, the power of the set $\mathcal{I}_\Phi(\tau, b)_\tau$ is generally bigger than 1. This is because there are some other possible incident angles that result in the same value of $s = v_a\tau$ (see Fig. 5). Considering Eq. (3), it means that all possible solutions ϕ_s for the given measurement result τ are contained in the set

$$\mathcal{A}_\Phi(\tau, b)_\tau = \left\{ \phi_i = \arcsin \frac{v_a\tau + n_i\lambda}{b} : n_i \in \mathcal{I}_\Phi(\tau, b)_\tau \right\}.$$

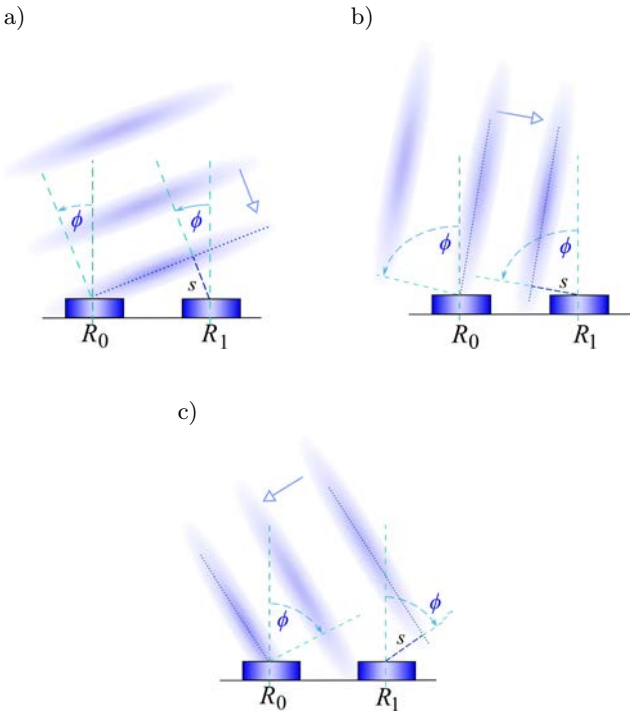

Fig. 5. Ambiguous results of the incident angle ϕ for the same value s.

Using the same argumentation that was applied for introducing the representation of the azimuth angle values of the set $\mathcal{I}_\Phi(\phi, b)_\phi$, the set $\mathcal{A}_\Phi(\tau, b)_\tau$ will also be denoted as $\mathcal{A}_\Phi(\phi, b)_\phi$. In the sense of this notation, it is worth noticing that

$$\forall\phi \in \Phi, \qquad \phi \in \mathcal{A}_\Phi(\phi, b)_\phi. \tag{5}$$

It is also convenient to define a set of all possible solutions of Eq. (3) for the entire Φ as follows

$$\mathcal{A}^\Phi(b) = \{\mathcal{A}_\Phi(\phi, b)_\phi : \phi \in \Phi\}.$$

5. Ambiguity removal

The notation introduced in the previous section allows the case for which a unique solution of Eq. (3) is determined to be described as follows

$$b \le \frac{\lambda}{2} \;\wedge\; \forall\mathcal{A}_\Phi(\phi, b)_\phi \in \mathcal{A}^\Phi(b), \quad |\mathcal{A}_\Phi(\phi, b)_\phi| = 1, \tag{6}$$

where $|\mathcal{A}(.)|$ is the power of the set $\mathcal{A}(.)$. When $\Phi = \left(-\frac{\pi}{2}, \frac{\pi}{2}\right)$, the opposite case can be expressed in the way presented below

$$b > \frac{\lambda}{2} \;\wedge\; \exists\mathcal{A}_\Phi(\phi, b)_\phi \in \mathcal{A}^\Phi(b), \quad |\mathcal{A}_\Phi(\phi, b)_\phi| > 1. \tag{7}$$

If $\frac{\lambda}{2} < b < \lambda$, then it is possible to restrict the set Φ to $\Phi_{\text{res}} = (-\phi_{\text{res}}, \phi_{\text{res}})$ where

$$\phi_{\text{res}} = \arcsin \frac{\lambda}{2b}.$$

For the set Φ_{res}, the conditions (6) and (7) can be reformulated as follows

$$b > \frac{\lambda}{2} \ \wedge \ \forall \phi \in \Phi_{\text{res}}, \quad |\mathcal{A}_\Phi(\phi, b)_\phi| = 1,$$

and

$$b > \frac{\lambda}{2} \ \wedge \ \forall \phi \in \left(-\frac{\pi}{2}, \frac{\pi}{2}\right) \backslash \Phi_{\text{res}}, \quad |\mathcal{A}_\Phi(\phi, b)_\phi| > 1.$$

The same can be said about sets $\mathcal{I}_\Phi(\phi, b)_\phi$. Due to the effective sensitivity ranges of the popular ultrasonic transducers being no wider than $[-70°, 70°]$, the examples presented in further analysis are restricted to that range. Therefore, it is assumed that $\Phi = [-70°, 70°]$. The conclusions are also true for wider ranges up to $\left(-\frac{\pi}{2}, \frac{\pi}{2}\right)$.

Popular piezoelectric transducers operate at the frequency of 40 kHz. In normal conditions, the length of this wave is about 8.7 mm. Thus, for $\phi_{\text{res}} = 70°$, the corresponding value of b is 4.6 mm.

To visualize how the power of sets $\mathcal{A}(.)$ is changed in relation to a value of b and, in this context, what ϕ_{res} means, two diagrams are shown in Fig. 6. They represent sets $\mathcal{A}^\Phi(b)$ for $b = 11$ mm and $b = 15$ mm respectively. The diagrams show the relation between the real azimuth angle ϕ and members ϕ_i of $\mathcal{A}_\Phi(\phi, b)_\phi$. When choosing e.g. the azimuth angle $\phi = -20°$ using the diagram in Fig. 6a, the following is obtained

$$\mathcal{A}_\Phi(-20°, 11 \text{ mm})_\phi = \{-22°, 20°\}.$$

a)

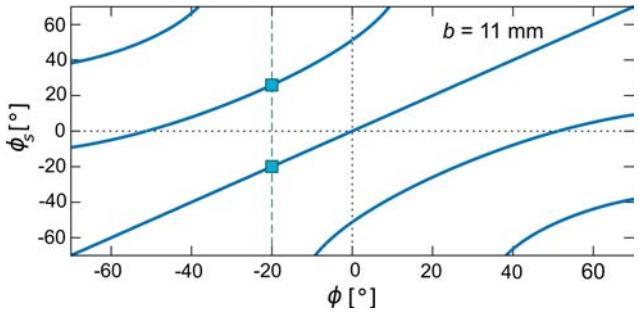

b)

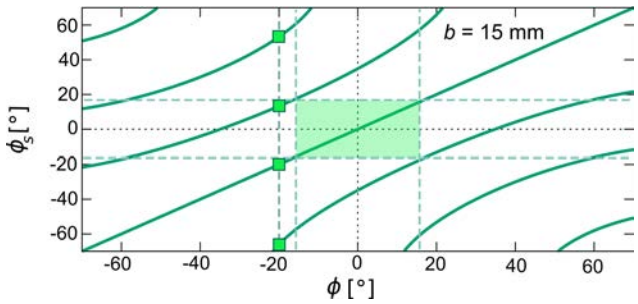

Fig. 6. Values of possible solutions ϕ_s of Eq. (2) in relation to the values of the incident angle ϕ for the size of the gap b equal to: a) 11 mm, b) 15 mm.

In the second diagram in Fig. 6b, it is

$$\mathcal{A}_\Phi(-20°, 15 \text{ mm}) = \{-48°, -11°, 20°, 68°\}.$$

It is worth noting that proper values ϕ_i, which belong to each $\mathcal{A}_\Phi(.)_\phi$, are aligned along the diagonals of the diagrams because $\phi_i = \phi$.

In the diagram presented in Fig. 6b, the restricted set of Φ marked by the darker rectangle is also shown. In the area of this rectangle, a unique solution of Eq. (2) can be found. For $b = 15$ mm, the value of ϕ_{res} is about 16.9°. As was said before, the angular sensitivity of a real sonar system is much higher. For the sonar system used in the experiments presented in Sec. 9, its range of sensitivity was about $[-50°, 50°]$. In this case, the corresponding value b for $\phi_{\text{res}} = 50°$ is 5.7 mm. Unfortunately, commercially available popular piezoelectric transducers do not make it possible to meet this condition. Their common diameters are 10 mm, 12 mm, 14 mm, and 16 mm. To overcome the problem of ambiguity, instead of a single receiver pair, two pairs that have different inter-distances can be used. They can be integrated into a single system of three receivers (see Fig. 7). For simplicity, it is assumed that the sensitivity ranges of all receivers are the same. In other cases, a common part of all receiver sensitivity ranges can be set as the range of the entire receiver system. Considering the two receiver pairs, namely (R_0, R_1) and (R_1, R_2), for a given azimuth ϕ, the two sets $\mathcal{A}_\Phi(\phi, b_{01})_\phi$ and $\mathcal{A}_\Phi(\phi, b_{12})_\phi$ of the possible solutions are obtained. Because of condition (5),

$$\forall \phi \in \Phi, \qquad \phi \in \mathcal{A}_\Phi(\phi, b_{01})_\phi \cap \mathcal{A}_\Phi(\phi, b_{12})_\phi. \tag{8}$$

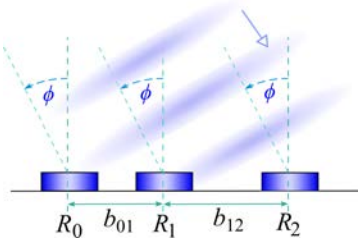

Fig. 7. Two pairs of receivers integrated into a single system of three transducers.

In other words, it means that for all $\phi \in \Phi$ exist $n_i \in \mathcal{I}_\Phi(\phi, b_{01})_\phi$ and $n_j \in \mathcal{I}_\Phi(\phi, b_{12})_\phi$ such that

$$\phi = \arcsin \frac{v_a \tau_{01} + n_i \lambda}{b_{01}} \ \wedge \ \phi = \arcsin \frac{v_a \tau_{12} + n_j \lambda}{b_{12}}. \tag{9}$$

Because $\Phi \subseteq \left(-\frac{\pi}{2}, \frac{\pi}{2}\right)$, the relation (9) is equivalent to

$$\sin \phi = \frac{v_a \tau_{01} + n_i \lambda}{b_{01}} \ \wedge \ \sin \phi = \frac{v_a \tau_{12} + n_j \lambda}{b_{12}}. \tag{10}$$

When

$$\forall \phi \in \Phi, \qquad |\mathcal{A}_\Phi(\phi, b_{01})_\phi \cap \mathcal{A}_\Phi(\phi, b_{12})_\phi| = 1, \tag{11}$$

then having τ_{01} and τ_{12} the computation of the azimuth angle ϕ means to determine the sets $\mathcal{A}_\Phi(\tau_{01}, b_{01})_\tau$ and $\mathcal{A}_\Phi(\tau_{12}, b_{12})_\tau$ and find their common part, because

$$\mathcal{A}_\Phi(\tau_{01}, b_{01})_\tau \cap \mathcal{A}_\Phi(\tau_{12}, b_{12})_\tau = \{\phi\}. \tag{12}$$

It shows that the crucial point is to choose such b_{01} and b_{12} for which the condition (11) is met for all $\phi \in \Phi$. When b_{01} and $b_{12} > \frac{\lambda}{2}$, it is evident that it must not be $b_{01} = b_{12}$. Because otherwise, the condition (7) is fulfilled and, therefore, there is a subset of Φ or the entire set Φ whose values ϕ do not meet the condition (11).

Unfortunately, it can be expected that $b_{01} = b_{12}$ is not the only case for which the condition (11) is not fulfilled. Therefore, it is essential to find a more general rule that will make it possible to omit these cases. This rule should allow the best configuration of the b_{01} and b_{12} values to be found. In the sense of anticipated errors of measurements, the best configuration should enable the receiver system to have the largest minimal distance between the incorrect values of the azimuth angle that belong to sets $\mathcal{A}_\Phi(.)$ of both receiver pairs. To explain what the minimal distance means, two integrated receiver pairs will be considered. Their inter-distances b_{01} and b_{12} are the same as the ones analysed in the example shown in Fig. 6. For these two pairs, the diagrams presented in Fig. 6 should be combined. Its result is presented in Fig. 8. It is worth noting that their only common part are diagonals that contain the correct solutions of Eq. (3).

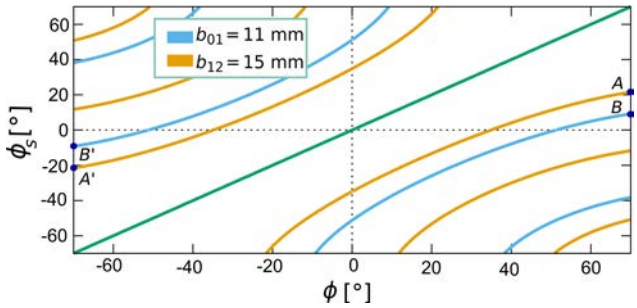

Fig. 8. The diagram of the combined solution sets determined for two cases of gap b equal to 11 mm and 15 mm.

The minimal distance between ambiguous solutions of both pairs for this particular case is the distance between points A and B. The same distance is on the opposite side of the diagram between points A' and B' and is equal to about 12°. Formally, this distance for a specific azimuth angle ϕ can be defined as follows

$$D_\phi(b_{01}, b_{12}) = \min_{\substack{\phi_{p_i} \in \mathcal{A}_\Phi(\phi, b_{01})_\phi, \\ \phi_{p_j} \in \mathcal{A}_\Phi(\phi, b_{12})_\phi, \\ \phi_{p_i} \neq \phi \wedge \phi_{p_j} \neq \phi}} |\phi_{p_i} - \phi_{p_j}|. \tag{13}$$

It is important to note that in Eq. (13) the case when ϕ_{p_i} and ϕ_{p_j} are simultaneously equal ϕ must be excluded, because this is the proper solution. In such a case, the distance is always 0. Using Eq. (13), the distance for the entire set Φ is defined by the following formula

$$D_\Phi(b_{01}, b_{12}) = \min_{\phi_i \in \Phi} D_{\phi_i}(b_{01}, b_{12}). \tag{14}$$

Because $\Phi \subseteq \left(-\frac{\pi}{2}, \frac{\pi}{2}\right)$ and, therefore, the relation (9)is equivalent to (10), it is much more useful and convenient to analyse this type of distance in the space of sinus values of the azimuth ϕ instead of analysing it directly in the space of angles. Moreover, it is much simpler, because in the space of sinus values, the curves from Fig. 8 are transformed into the sinus lines presented in Fig. 9. They are shifted against each other along the axis OY. This is the simple conclusion inferred from (3). Each such line is shifted by $\frac{n_i \lambda}{b}$ where b is, in this case, equal to b_{01} or b_{12} respectively. In the same way, instead of using sets of possible solutions like

$$\mathcal{A}_\Phi(\phi, b)_\phi = \{\phi_{p_1}, \ldots, \phi_{p_k}\},$$

it is much more convenient to present them in the space of sinus value

$$\mathcal{A}^{\sin}_\Phi(\phi, b)_\phi = \{\sin\phi_{p_1}, \ldots, \sin\phi_{p_k}\} = \{s_{\phi,1}, \ldots, s_{\phi,k}\},$$

where the notation $s_{\phi,i}$ is used for emphasizing that this is a sinus value of i-th solution of Eq. (3) while the incident angle is ϕ. The notation $\mathcal{A}^{\sin}_\Phi(\tau, b)_\tau$, which is analogous to the previous one $\mathcal{A}_\Phi(\tau, b)_\tau$, will be used for emphasizing that sinus values are determined by τ. When the error of τ measurement is zero, the sets $\mathcal{A}^{\sin}_\Phi(\phi, b)_\phi$ and $\mathcal{A}^{\sin}_\Phi(\tau, b)_\tau$ are the same.

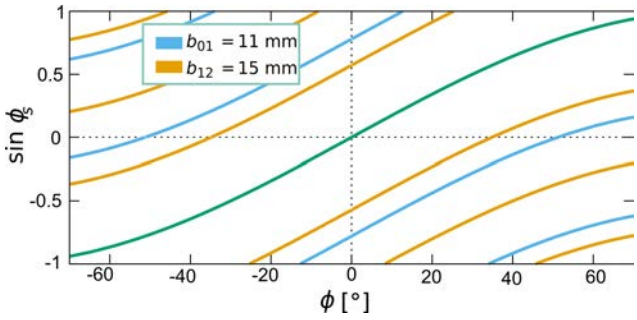

Fig. 9. The diagram of sinus values of the combined solution sets determined for two cases of gap b equal to 11 mm and 15 mm.

Using the same schema of definition of D_Φ, the measure of the minimal distance of the ambiguous solution can be defined in the space of sinus values as follows

$$D^{\sin}_\phi(b_{01}, b_{12}) = \min_{\substack{s_{\phi,i} \in \mathcal{A}^{\sin}_\Phi(\phi, b_{01})_\phi, \\ s_{\phi,j} \in \mathcal{A}^{\sin}_\Phi(\phi, b_{12})_\phi, \\ s_{\phi,i} \neq \sin\phi \wedge s_{\phi,j} \neq \sin\phi}} |s_{\phi,i} - s_{\phi,j}| \tag{15}$$

and

$$D^{\sin}_\Phi(b_{01}, b_{12}) = \min_{\phi_i \in \Phi} D^{\sin}_{\phi_i}(b_{01}, b_{12}). \tag{16}$$

This formula is difficult to calculate. Fortunately, it can be radically simplified (see Theorem 1 in Appendix).

The relation between the values of $D_{\Phi}^{\sin}$ and inter-distances b_{01} and b_{12} cannot be expressed in a simple analytic form because it is highly nonlinear. However, by performing numerical computations it is possible to visualize it. In Fig. 10, diagrams are presented that show the distribution of $D_{\Phi}^{\sin}$ for $b_{01}, b_{12} \in [10, 30\text{ mm}]$ and $\Phi = [-70°, 70°]$. It was mentioned before that when b_{01} and b_{12} are equal to each other, this approach cannot work. In the diagrams, it is manifested by a kind of *valley* along the diameter determined by the condition $b_{01} = b_{12}$. Its bottom is at the zero level. This valley is not the only place where the value zero is reached. In the diagram, there are quite a lot of these kinds of valleys. Their location determines a more general feature, which is stated in Theorem 2 in Appendix. In short, if $D_{\Phi}^{\sin}(b_{01}, b_{12}) = 0$, then there exist $k_i, k_j \in \mathbf{I}$ such that the following condition is met

$$k_j b_{01} = k_i b_{12}.$$

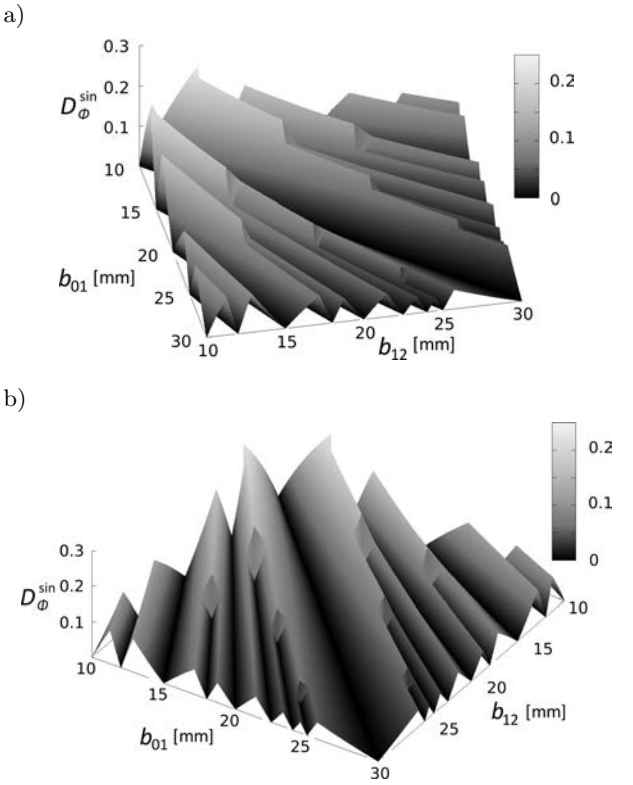

Fig. 10. The dependence of $D_{\Phi}^{\sin}$ on the values of b_{01} and b_{12} for $\Phi = [-70°, 70°]$. In order to get a better expression of value changes, the diagram is presented from two points of view.

The diagram in Fig. 10 shows that there are some discontinuities that start bifurcations and new valleys. It is easier to notice it when this diagram is presented in a bird-eye view (see Fig. 11). This clearly shows that some ridges turn into valleys. In the diagram presented in Fig. 11, these places are

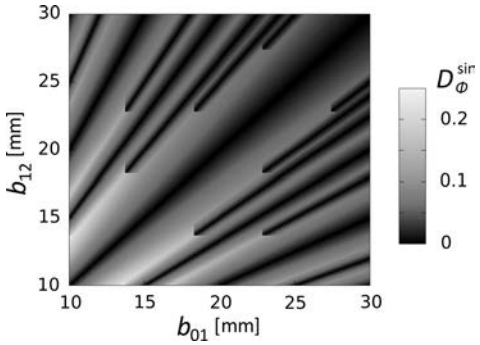

Fig. 11. The bird-eye view of the surface defined by the dependence of $D_{\Phi}^{\sin}$ on the values of b_{01} and b_{12} for $\Phi = [-70°, 70°]$.

located at the points $(13.05, 17.40)$, $(13.05, 21.75)$, $(17.40, 21.75)$, $(21.75, 26.10)$ and their symmetrical images, namely $(17.40, 13.05)$, $(21.75, 13.05)$, $(21.75, 17.40)$, $(26.10, 21.75)$. The locations of the discontinuity can be determined by using Theorem 3 included in Appendix. The characteristic corner-like shape of discontinuity regions is also explained there.

It has to be noted that the diagram of $D_{\Phi}^{\sin}$ strongly depends on the range of Φ. The smaller the range of Φ, the smaller the number of ambiguous solutions. This results in a smaller number of valleys and ridges. An example of such a change is shown in Fig. 12. The range of Φ is restricted to $[-50°, 50°]$. This range is

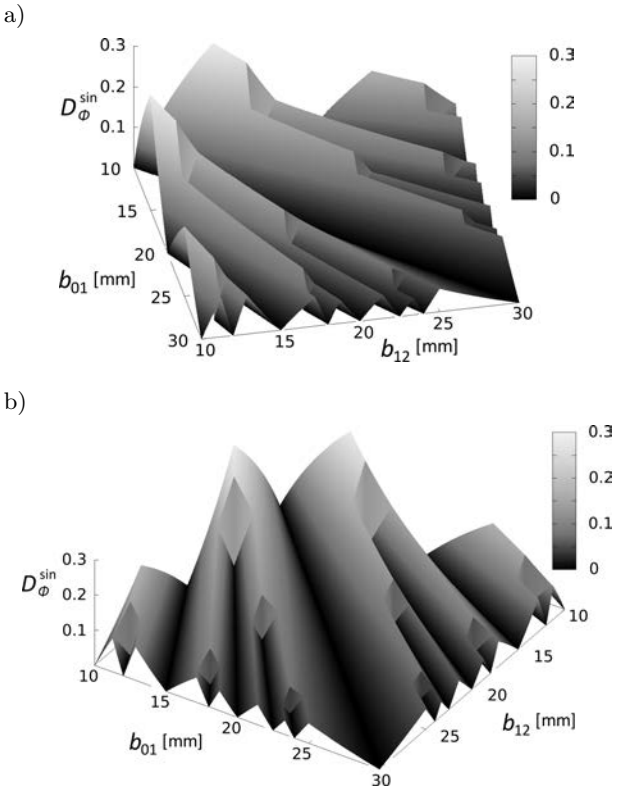

Fig. 12. Two views of the diagram of $D_{\Phi}^{\sin}$ in relation to b_{01} and b_{12} for $\Phi = [-50°, 50°]$.

more reasonable in the sense of the parameters of the piezoelectric transducers that are available on the market. Therefore, in the further part of this paper it will be used as the reference range for this kind of diagrams.

6. Robustness

Assuming for simplicity that errors of time period measurement can be approximated by the same value $\Delta\tau$ for each receiver pair, an error of sinus value determination for the pairs $P_{01} = (R_0, R_1)$ and $P_{12} = (R_1, R_2)$ are respectively

$$\Delta_{01}(\sin\phi) = \frac{v_a\Delta\tau}{b_{01}}, \qquad \Delta_{12}(\sin\phi) = \frac{v_a\Delta\tau}{b_{12}}. \tag{17}$$

Considering errors of echo signal detection performed by each receiver and assuming that errors can be approximated by the same value $\Delta\mathrm{t}$, then

$$\Delta\tau = 2\Delta\mathrm{t}. \tag{18}$$

This is because

$$\tau_{01} = \mathrm{t}_1 - \mathrm{t}_0, \qquad \tau_{12} = \mathrm{t}_2 - \mathrm{t}_1,$$

where t_0, t_1, t_2 are measurements of time of the signal detection performed by receivers R_0, R_1, and R_2, respectively.

The errors of b_{01} and b_{12} are systematic errors and can be taken into account during a calibration procedure. Therefore, they are not considered here. In the further part of this paper, a shorter notation of the expressions (17) will be used, namely: $\Delta_{s,01}$ and $\Delta_{s,02}$.

Taking into account these types of errors, sets $\mathcal{A}^{\sin}_{\Phi}(.)_\phi$ of discrete sinus values should be transformed into sets of value ranges. Such a set is defined as follows

$$\mathcal{A}^{\sin\Delta}_{\Phi}(\phi, b_{ij})_\phi = \{[s_{\phi,k} - \Delta_{s,ij}, s_{\phi,k} + \Delta_{s,ij}] : s_{\phi,k} \in \mathcal{A}^{\sin}_{\Phi}(\phi, b_{ij})_\phi\}.$$

Then, the condition (12), which guarantees finding the proper solution in the entire considered range of Φ, is transformed into the form

$$\begin{aligned} &\forall\phi\in\Phi \quad \exists\,[s_x, s_y] \subseteq [-1, 1], \\ &\quad \mathcal{A}^{\sin\Delta}_{\Phi}(\phi, b_{b_{01}})_\phi \cap \mathcal{A}^{\sin\Delta}_{\Phi}(\phi, b_{b_{12}})_\phi \\ &\quad = \{[s_x, s_y]\} \;\wedge\; \sin\phi \in [s_x, s_y], \end{aligned} \tag{19}$$

where $[s_x, s_y]$ is a common part of value ranges which belongs to $\mathcal{A}^{\sin\Delta}_{\Phi}(\phi, b_{b_{01}})_\phi$ and $\mathcal{A}^{\sin\Delta}_{\Phi}(\phi, b_{b_{12}})_\phi$. It causes a crucial question to arise. What is the limit of error $\Delta\mathrm{t}$ for the given receivers' configuration that makes it possible to meet the condition (19)?

In order to answer this question it is necessary to find the minimal value of $D^{\sin}_{\Phi}$ for which the condition (19) is met. Then, using this value, $\Delta\mathrm{t}$ can be determined.

Considering the graphical interpretation, lines that represent possible solutions (see Fig. 9) turn into stripes (see Fig. 13) whose width along the OY axis is $2\Delta_{s,01}$ and $2\Delta_{s,12}$ respectively. It is simple to notice that the maximal distance between points belonging to two stripes, which represent a proper solution of the receiver pairs (R_0, R_1) and (R_0, R_1), is $\Delta_{s,01} + \Delta_{s,12}$. This distance is reached when the azimuth values determined by measurements are at opposite borders of the stripes. This is because the stripes partially overlap each other along the common sinus line. Such a case is represented by points P_a and P_b in Fig. 13. In this sense, these points represent acceptable solutions when their distance is lower or equal to $\Delta_{s,01} + \Delta_{s,12}$. For this reason, to separate two false solutions of two receiver pairs, the distance between sinus values located at borders in regions determined by possible error values (see points P'_a and P'_b in Fig. 13) must be bigger than $\Delta_{s,01} + \Delta_{s,12}$. Therefore, the distance between the sinus values that are not corrupted by errors must be twice as big. It means that the necessary and sufficient condition for the given inter-distances b_{01} and b_{12} is

$$D^{\sin}_{\Phi}(b_{01}, b_{12}) > 2(\Delta_{s,01} + \Delta_{s,12}). \tag{20}$$

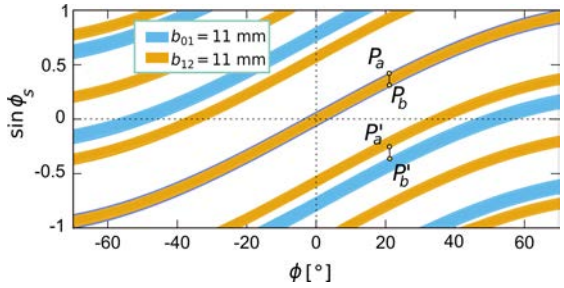

Fig. 13. The diagram of sinus values, which includes a range of approximated maximal measurement errors.

Taking into account Eq. (17), the relation (20) can be transformed into the form

$$\frac{b_{01}b_{12}D^{\sin}_{\Phi}(b_{01}, b_{12})}{2v_a(b_{01} + b_{12})} > \Delta\tau. \tag{21}$$

Thus, for the given b_{01} and b_{12} values, it determines the upper limit $\overline{\Delta}\tau_\Phi$ of the acceptable error $\Delta\tau$ of period measurement determined for the entire range of Φ

$$\overline{\Delta}\tau_\Phi = \frac{b_{01}b_{12}D^{\sin}_{\Phi}(b_{01}, b_{12})}{2v_a(b_{01} + b_{12})}. \tag{22}$$

Because of Eq. (18), the upper limit of the acceptable error $\Delta\mathrm{t}$ of the time measurement is

$$\overline{\Delta}\mathrm{t}_\Phi = \frac{1}{2}\overline{\Delta}\tau_\Phi. \tag{23}$$

When a bigger error $\overline{\Delta}\mathrm{t}_\Phi$ is acceptable, the system is more robust. In this sense, $b^\star_{01}$ and $b^\star_{12}$ determine the

best configuration of such a system when they refer to the biggest value $\overline{\Delta}\mathrm{t}^{\star}_{\Phi}$. Regarding the relations (22) and (23), it means that

$$\overline{\Delta}\mathrm{t}^{\star}_{\Phi} = \frac{1}{4v_a}\frac{b^{\star}_{01}b^{\star}_{12}}{b^{\star}_{01}+b^{\star}_{12}}D^{\sin}_{\Phi}(b^{\star}_{01},b^{\star}_{12}) = \frac{1}{4v_a}\max_{b_{01},b_{12}}\frac{b_{01}b_{12}}{b_{01}+b_{12}}D^{\sin}_{\Phi}(b_{01},b_{12}).$$

The relation between $\overline{\Delta}\mathrm{t}_{\Phi}$ and the values of b_{01} and b_{12} is presented on the diagrams shown in Fig. 14. The surface determined by Eq. (22) is shown from two points of view to give better intuition about this relation. Its general feature is that bigger values of b_{01} and b_{12} correspond to smaller values of $\overline{\Delta}\mathrm{t}_{\Phi}$.

a)

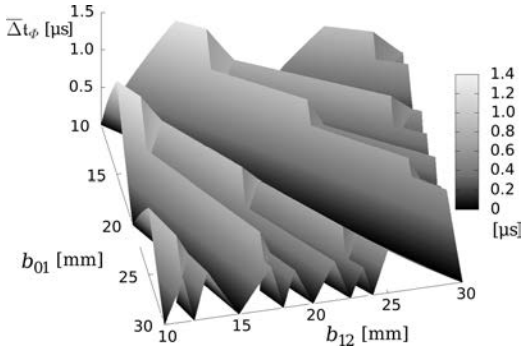

b)

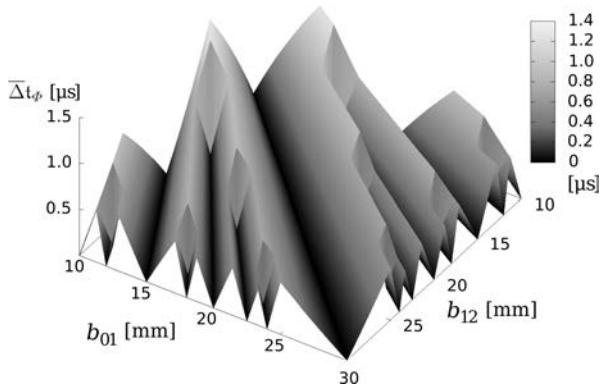

Fig. 14. Minimal distance between ambiguous solutions expressed in time of the upper limit of the acceptable error $\overline{\Delta}\mathrm{t}_{\Phi}$ for $\Phi = [-50^{\circ}, 50^{\circ}]$. The distance is shown as a function of length of baselines b_{01} and b_{12}.

For the analysed range of b_{01} and b_{12} values, the maximal error $\overline{\Delta}\mathrm{t}^{\star}_{\Phi}$ is equal to 1.3 μs and is obtained for $b^{\star}_{01}$ = 11.2 mm and $b^{\star}_{12}$ = 16.8 mm. The equivalent solution is $b^{\star}_{01}$ = 16.8 mm and $b^{\star}_{12}$ = 10.2 mm.

The obtained value of $\overline{\Delta}\mathrm{t}^{\star}_{\Phi}$ is rather small. In order to improve it, a reduction of the inter-distance b_{01} or b_{12} should be considered. In Fig. 15, the diagrams are presented in which the range of the inter-distance b_{01} was started from the value 0.01 mm. This time, the best configuration is for $b^{\star}_{01}$ = 5.6 mm and $b^{\star}_{12}$ = 10 mm.

a)

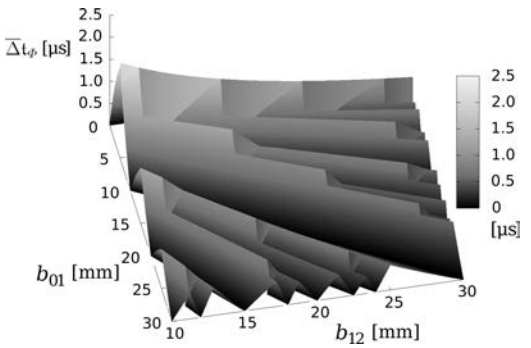

b)

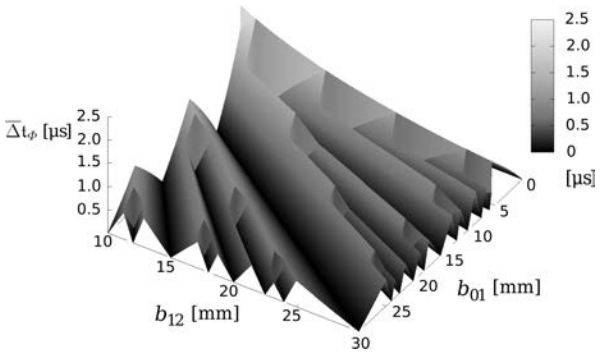

Fig. 15. Minimal distance between ambiguous solutions expressed in time of an acceptable measurement error $\overline{\Delta}\mathrm{t}_{\Phi}$ ($\Phi = [-50^{\circ}, 50^{\circ}]$) for the extended range of values of b_{01}.

The value of the acceptable error $\overline{\Delta}\mathrm{t}^{\star}_{\Phi}$ of the time measurement is 2.2 μs. Because of Eq. (23), the value of the acceptable error $\overline{\Delta}\tau^{\star}_{\Phi}$ of the period measurement is 4.4 μs. Comparing the value of $\overline{\Delta}\tau^{\star}_{\Phi}$ with the period of the signal, which is 25 μs, the tolerance of an error measurement is about 18% of the signal period.

Taking into account the previous assumption that a signal wave is a planewave and is propagated across a plain determined by the receivers' acoustic axes, it is possible to arrange a system of three receivers in a slightly different way. Instead of putting them along a single line, one of them can be moved a bit above (see Fig. 16). This allows an effective distance in a horizontal line to be reduced below their diameters. In this way, it is possible to reduce b_{01} to the distance 4.4 mm.

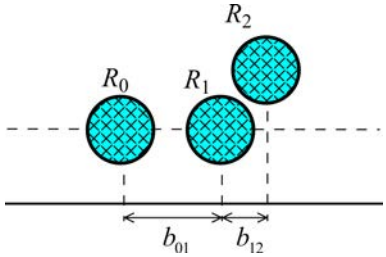

Fig. 16. Arrangement of three receivers with a reduced horizontal gap.

When $s_{\tau_{01}}$ and $s_{\tau_{12}}$ are determined and the common part of their surroundings, i.e. $[s_{\tau_{01}} - \Delta_{s,01}, s_{\tau_{01}} + \Delta_{s,01}]$ and $[s_{\tau_{12}} - \Delta_{s,12}, s_{\tau_{12}} + \Delta_{s,12}]$, respectively, meet the condition (19), then the final sinus value should be computed. In order to do this, errors $\Delta_{s,01}$ and $\Delta_{s,12}$ should be taken into account. Their values can be interpreted as factors of confidence that the obtained results refer to the real ones. Thus, the confidence measure can be defined in the following way

$$p_{01} = \frac{\Sigma_\Delta - \Delta_{s,01}}{2\Sigma_\Delta}, \qquad p_{12} = \frac{\Sigma_\Delta - \Delta_{s,12}}{2\Sigma_\Delta},$$

where

$$\Sigma_\Delta = \Delta_{s,01} + \Delta_{s,12}.$$

The consequence of such a definition is

$$p_{01} + p_{12} = 1.$$

Taking this into account, the mean value of the obtained results is computed as follows

$$\mu_s = p_{01} s_{\tau_{01}} + p_{12} s_{\tau_{12}}.$$

In a similar way, a squared divergence can be determined

$$\sigma_s^2 = p_{01}(s_{\tau_{01}} - \mu_s)^2 + p_{12}(s_{\tau_{12}} - \mu_s)^2.$$

This computational procedure was described for the receiver system consisting of two receiver pairs. It is clear that it can be extended to any number of such pairs.

7. Multi-pair receiver system

Until now, when analysing the system consisting of three receivers, the single subsystem consisting of two pairs $\{(R_0, R_1), (R_1, R_2)\}$ was considered. However, there are two other subsystems: $\{(R_0, R_1), (R_0, R_2)\}$ and $\{(R_0, R_2), (R_1, R_2)\}$. Taking them into account, condition (19) can be rewritten in the form

$$\begin{aligned} &\forall \phi \in \Phi \quad \exists\ [s_x, s_y] \subseteq [-1, 1], \\ &\quad \mathcal{A}_\Phi^{\sin\Delta}(\phi, b_{b_{01}})_\phi \cap \mathcal{A}_\Phi^{\sin\Delta}(\phi, b_{b_{12}})_\phi \\ &\quad \cap\, \mathcal{A}_\Phi^{\sin\Delta}(\phi, b_{b_{02}})_\phi = \{[s_x, s_y]\} \\ &\quad \wedge\ \ \sin\phi \in [s_x, s_y]. \end{aligned} \tag{24}$$

As was said at the end of the previous section, computing of μ_s and σ_s can be extended to this case.

In (Kreczmer, 2018), it was shown that the accuracy of the receiver system was increased by including these new receiver pairs. A further increase of accuracy can be obtained by adding a fourth receiver. In this way, six subsystems is obtained. The size of a sonar is also increased by adding a receiver. In consequence, it is harder to meet the assumption that a received wave is flat. Four receivers seem to be a good compromise between the sonar size and its accuracy of azimuth angle determination. The final geometrical arrangement of four receivers is shown in Fig. 17. Considering the range of azimuth angles $\Phi = [-50°, 50°]$, due to simulations it was found that the acceptable error $\overline{\Delta}\mathrm{t}_\Phi$ of the time measurement for this receiver arrangement is 1.56 μs. It gives SNR of about 8.4 dB. The acceptable error $\overline{\Delta}\mathrm{t}_\Phi$ is lower than the 2.2 μs found in the previous section for the optimal arrangement of three receivers. The main reason for this is that the horizontal distance between receivers R_2 and R_3 is smaller that the optimal one.

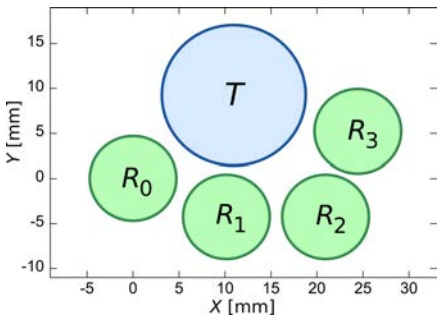

Fig. 17. Geometrical arrangement of sonar receivers and a transmitter.

8. Temperature dependence

Among the atmospheric parameters, namely: temperature, pressure, humidity; the temperature affects the propagation of acoustic waves the most. Considering the range of temperature from −20°C up to 40°C, the speed of acoustic waves is changed from 319.1 m/s up to 354.9 m/s. This means that the wavelength of a signal of 40 kHz is changed from 7.98 mm up to 8.87 mm. In order to perform a more accurate error analysis for particular values of the azimuth angle ϕ, the interval Φ can be limited to the considered single value ϕ (i.e. $\Phi = [\phi]$). To emphasize this, the tolerated error of the time measurement for this case will be denoted as $\overline{\Delta}\mathrm{t}_\phi$. Considering the geometrical arrangement of sonar receivers presented in the previous section, for the temperature of 20°C, due to the performed simulations, it was found that $\overline{\Delta}\mathrm{t}_\phi$ is constant in a wide range of azimuth angles of signal arrival and is equal to 1.56 μs (see Fig. 18). In this case, this range is [−63.4°, 63.4°]. Changes of temperature cause that the width of this range is slightly decreased with a temperature from [−64.25°, 64.25°] for −20°C to [−62.88°, 62.88°] for 40°C. Nevertheless, this range is still far bigger than the ranges of sensitivity of most transducers. In summary, when $\Phi = [-62.88°, 62.88°]$ for the considered case, the value of $\overline{\Delta}\mathrm{t}_\Phi$ is not affected by temperature changes in the range [−20°C, 40°C].

The presented insensitivity to temperature changes is not an inherent feature of the presented approach.

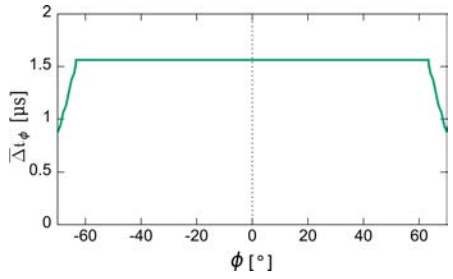

Fig. 18. Values of tolerated error $\overline{\Delta}t_\phi$ of the time measurement in relation to the azimuth angle of the direction of signal arrival for the air temperature of 20°C.

It strongly depends on the inter-distances between receivers. In order to explained this, it is convenient to consider a system consisting of three receivers R_0, R_1 and R_2. The diagram presented in Fig. 19 shows how $\overline{\Delta}t_\Phi$ depends on inter-distances b_{01} and b_{12}. The change of wavelength caused by temperature change does not cause any significant variation of the height of ridges. The only changes that are observed are the positions of bifurcations. In the example presented in Fig. 19 two diagrams at the bird-eye view are shown. They refer to the temperatures of 32°C and 2°C respectively. When the inter-distances of receivers are b_{01} = 15.5 mm and b_{12} = 10.34 mm (see the point A in Fig. 19), then the acceptable error $\overline{\Delta}t_\Phi$ is 1.25 μs. It is the same in the temperatures of 2°C and 32°C. However, this kind of stability is lost when the selected inter-distances are b_{01} = 16.75 mm and b_{12} = 11.16 mm (see the point B in Fig. 19). For the temperature of 32°C, it works properly and $\overline{\Delta}t_\Phi$ = 1.25 μs. But for the temperature of 2°C it fails because $\overline{\Delta}t_\Phi$ is reduced to 0.003 μs. It is worth noting that this change is rapid, which is due to the discontinuity of the bifurcation.

a)

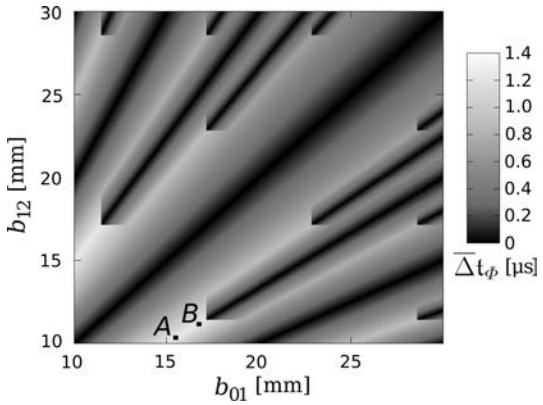

b)

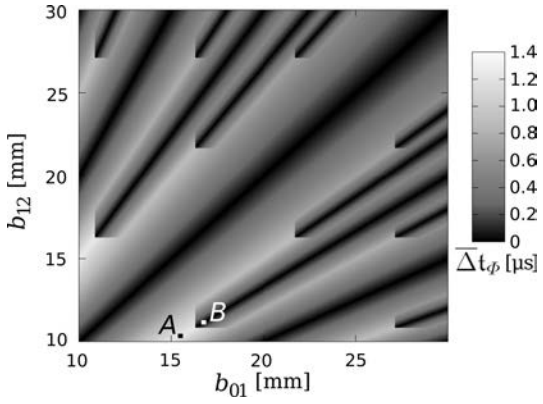

Fig. 19. Impact of temperature change on acceptable errors of time measurements for $\Phi = [-50°, 50°]$ and the temperature T: a) +32°C, b) +2°C.

9. Experiments

In the experiments, a sonar module was used (see Fig. 20a) for which the geometry was described in Sec. 7. The sonar is equipped with a single transmitter BPU-1640T0AH12 and four MA40S4R receivers. All ultrasonic transducers are controlled by the module (Kabała, Wnuk, 2005), which exploits the microcontroller MC9S12A64. The sonar module was mounted on a rotating base (see Fig. 20b). Using it, measurements were performed for different sonar orientations.

a) b)

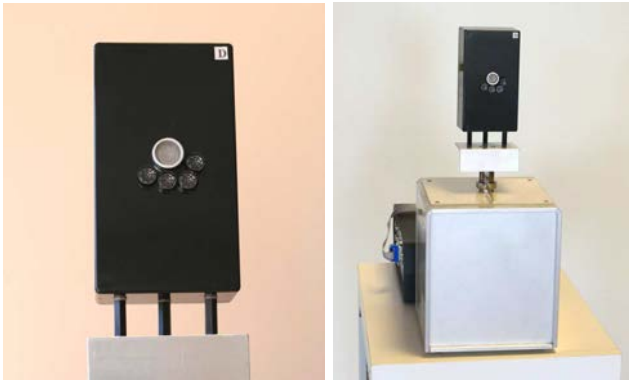

Fig. 20. a) A sonar module, b) a rotating base with a mounted sonar module.

In order to check the most important features of the proposed approach, measurements were performed for two types of objects, namely, a wall, and a post with a diameter of 25 mm. In each case, the determined azimuth angle ϕ was compared with the sonar orientation. The relation of the angle α of the sonar orientation and the azimuth angle ϕ of the echo arrival is presented in Fig. 21. For the wall case, in spite of an orientation of the sonar module transmitter, echos always arrive from the direction that is perpendicular to the surface of the wall. Therefore, for the ideal case when there are no measurement errors, the relation between ϕ and α should be as follows

$$\phi = -\alpha.$$

The same relation is also valid for the post.

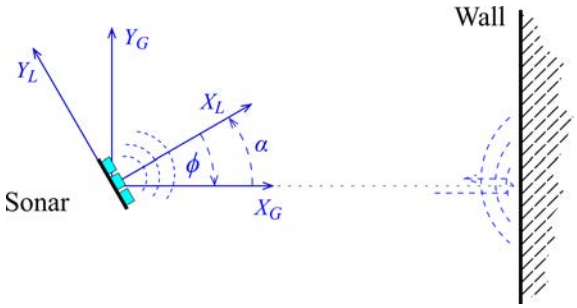

Fig. 21. Coordinate systems chosen for the experiment. The azimuth angle ϕ measured in the local coordinate system has an opposite sign to the rotation angle α measured in the global coordinate system.

For the presented approach to DOA determination, the wall case seems to be the most beneficial. By using the method of virtual sources (Kleeman, Kuc, 1995), it can be shown that the geometry of propagation of a wave reflected by a wall is the same as for the wave geometry of a transmitter placed at a distance twice as far as the distance to the wall. For the post, the same geometry is obtained when a transmitter is placed at a distance of an object. Because of this, the curvature of a wave reflected by a wall is much smaller than for other objects. It means that it is much closer to the assumption of this approach that a received wave is flat.

To perform measurements, the sonar was placed at a distance of 2.3 m from the wall (see Fig. 22). The sonar orientation was changed in the range of $[-30°, 30°]$ by the step of 1°. The wall was correctly detected in the range of $[-23°, 26°]$. At each sonar orientation, the measurement and determination of ϕ were repeated 100 times. Next, the mean value of ϕ and its root mean square error were computed. The obtained relation between the azimuth ϕ of the DOA and the orientation angle α of the sonar module is presented in Fig. 23. Errors of azimuth ϕ determination turned out to be so small that in the scale of this diagram the calculated values seem to be perfectly arranged along the diagonal of the diagram. The bars of root mean squared deviation (RMSD) were also marked. Because of the small values of RMSD, they cannot be distinguished from the line of the diagonal. The values of RMSD are no bigger than 0.22° (see Fig. 24). The only exception is the result obtained at the right limit of the orientation range of wall visibility. For this orientation, the obtained measurements are very unstable. It causes that the RMSD of the determined azimuth ϕ is rapidly increased up to 3.75°. This is because of weak echo signals. In the diagram shown in Fig. 24, values $\Delta\phi$ of the errors of azimuth determination are also presented. They are no bigger than 0.5°.

Fig. 22. Location of the rotary base with the sonar module in relation to the wall.

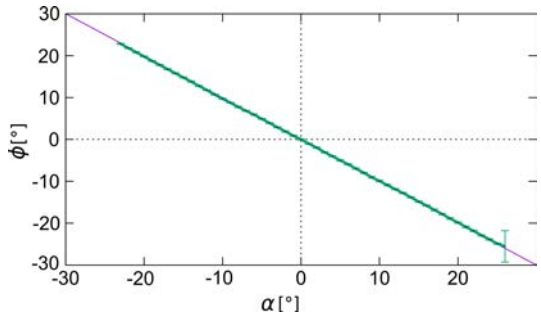

Fig. 23. Results of azimuth measurements for the wall at a distance of 2.3 m.

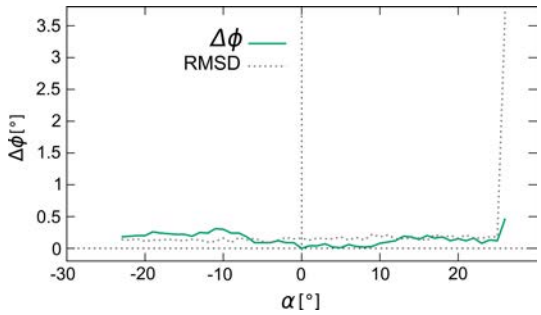

Fig. 24. Values of the root of mean squared deviation (RMSD) and azimuth error $\Delta\phi = |\phi - \alpha|$ obtained for the azimuth determination of the direction of the signal reflected from the wall.

In order to check the features of the presented method of DOA determination in a situation when a wave curvature is much bigger then for the wall case, a post with a diameter of 25 mm was used and placed at a distance of 0.8 m (see Fig. 25). The post was correctly detected in the range of sonar orientation $[-18°, 18°]$ (see Fig. 26). In Fig. 27, RMSD and values of error $\Delta\phi$ are presented. It can be noticed that their level is very similar to the case of the wall. Therefore, for this sonar, the change of wave curvature for these distances does not have a meaningful influence on the final result.

Fig. 25. Location of the rotary base with the sonar module in relation to the post.

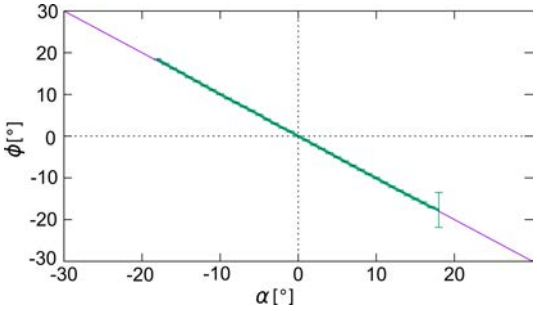

Fig. 26. Results of azimuth measurements for the post at a distance of 0.8 m.

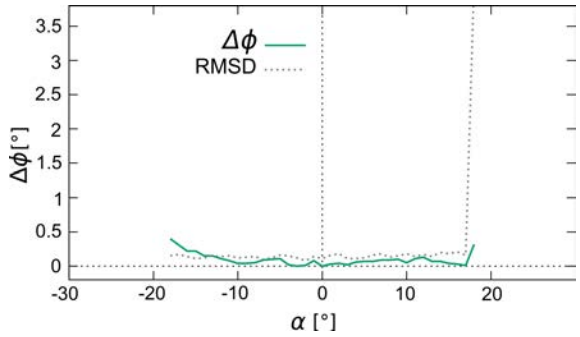

Fig. 27. Values of root of mean squared deviation (RMSD) and azimuth error $\Delta\phi = |\phi - \alpha|$ obtained for the azimuth determination of the direction of the signal reflected from the post.

The post is a source of much weaker echo signal than the wall. The sonar used in this experiment was able to detect the post at a distance of 3.4 m (see Fig. 28). For such a case, SNR increases due to the drop in signal strength. Nevertheless, the azimuth angle was still determined with a relatively small error of no more than about 2° (see Fig. 29).

Fig. 28. Location of the rotary base with the sonar module in relation to the post at a distance of 3.4 m.

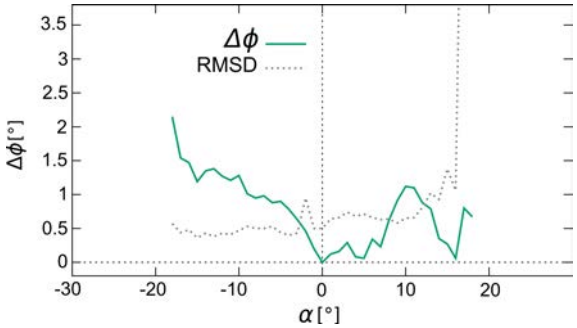

Fig. 29. Values of root of mean squared deviation (RMSD) and azimuth error $\Delta\phi = |\phi - \alpha|$ for the post at a distance of 3.4 m.

10. Conclusion

A very important advantage of the presented method is simplicity. The required computations are uncomplicated, and powerful microcontrollers are therefore not needed. Moreover, the measurement technique is also very simple. Because receivers have to be placed close to each other, the sonar module used in this technique can be compact in size. In spite of simplicity, the improvement of reliability of data interpretation compared with traditional ultrasonic range finders is dramatic. The increase of the number of receiver pairs made it possible to obtain a more accurate determination of the DOA. For four receivers, and all the pairs they create, the level of accuracy approximated by 3σ is still below 1°. For weak echos, σ is about 1°. The error of DOA determination increases up to 2°.

The disadvantage of the presented approach is its sensitivity to the mutual position of receivers. However, thanks to the theoretical analysis, it was possible to establish and formally prove the essential properties that allowed the selection of the best possible positions of the receivers. The choice made has also ensured the stability of the method for a wide range of air temperatures.

Using MEMS microphones, it is possible to arrange all receivers along a single line. Because of its axial

symmetry, two such systems placed perpendicular to each other can be used for obtaining data which allow azimuth and elevation angles, as well as distance to be determined. In this sense, the approach can be extended to the 3-D case in an almost straightforward way.

Appendix. Features of a narrow-band system of two receiver pairs

To be more precise, in this section, as well as in others, it is assumed that b_{01} and b_{12} are positive real numbers.

Theorem 1. Assuming that $\Phi = [\phi_{\min}, \phi_{\max}] \subset \left(-\frac{\pi}{2}, \frac{\pi}{2}\right)$, then

$$D^{\sin}_{\Phi}(b_{01}, b_{12}) = D^{\sin}_{\phi_{\min}}(b_{01}, b_{12}) = D^{\sin}_{\phi_{\max}}(b_{01}, b_{12}).$$

Proof: First, the case of $\phi_{\max}$ will be considered. For this angle, there exits such a number $n_{\max_{01}}$ that

$$\sin\phi_{\max} = \frac{v_a \tau_{01}(\phi_{\max}) + n_{\max_{01}}\lambda}{b_{01}}.$$

Because this value is the maximal one, all others obtained for $n_i \in \mathcal{I}_{\Phi}(\phi_{\max_{01}}, b_{12})_{\phi}$ are lower and uniformly placed in the range $[\sin\phi_{\min}, \sin\phi_{\max}]$. The interval between them is equal to $\frac{\lambda}{b_{01}}$. The same can be said about values related to the second receiver pair (R_1, R_2). The difference is that the interval is equal to $\frac{\lambda}{b_{12}}$. It is obvious that the minimal distance between the values of both receiver pairs must be lower or equal to $\min\left\{\frac{\lambda}{b_{01}}, \frac{\lambda}{b_{12}}\right\}$. The sets of sinus values for b_{01} and b_{12} create all possible combinations, and the set of distances which should be considered is

$$\begin{aligned}\boldsymbol{D}^{\sin}_{\Phi}(\phi_{\max}) = \Big\{\Delta^{\sin}_{ij} = |\sin\phi_i - \sin\phi_j| : \\ \phi_i \in \mathcal{A}_{\Phi}(\phi_{\max}, b_{01})_{\phi} \wedge \phi_j \in \mathcal{A}_{\Phi}(\phi_{\max}, b_{12})_{\phi} \\ \wedge (\phi_i \neq \phi_{\max} \wedge \phi_j \neq \phi_{\max}) \\ \wedge |\sin\phi_i - \sin\phi_j| \leq \min\left\{\frac{\lambda}{b_{01}}, \frac{\lambda}{b_{12}}\right\}\Big\}.\end{aligned}$$

Due to formula (15)

$$D^{\sin}_{\phi_{\max}}(b_{01}, b_{12}) = \min_{\Delta^{\sin}_{ij} \in \boldsymbol{D}^{\sin}_{\Phi}(\phi_{\max})} \Delta^{\sin}_{ij}.$$

For other choices of ϕ, it is simple to note that $\boldsymbol{D}^{\sin}_{\Phi}(\phi) \subseteq \boldsymbol{D}^{\sin}_{\Phi}(\phi_{\max})$. The reason is that the sinus lines of the incorrect solutions of (3) are symmetrically shifted in relation to the sinus line of the correct one (see Fig. 9). Thus, the set $\boldsymbol{D}^{\sin}_{\Phi}(\phi_{\max})$ contains the minimal value of the distance of sinus values computed for all possible solutions of Eq. (3) for both receiver pairs. Therefore

$$D^{\sin}_{\Phi}(b_{01}, b_{12}) = \min_{\Delta^{\sin}_{ij} \in \boldsymbol{D}^{\sin}_{\Phi}(\phi_{\max})} \Delta^{\sin}_{ij}.$$

In consequence,

$$D^{\sin}_{\Phi}(b_{01}, b_{12}) = D^{\sin}_{\phi_{\max}}(b_{01}, b_{12}).$$

Considering the second case of $\phi_{\min}$, it is worth noting that the diagram presented in Fig. 9 possesses some kind of symmetry. As was said before, the sinus lines of the incorrect solutions of Eq. (3) are symmetrically shifted in relation to the sinus line of the correct one. Since the limitation of the considered range of angles also limits the values of sines that correspond to these angles, then the number of sinus curves near the left and right limits are the same. An example of such a situation is shown in Fig. 30. For the sake of clarity, only one set of shifted sine curves has been used. For this reason, an analogous line of reasoning may be used for the case of $\phi_{\min}$, in relation to that which was presented for the case of $\phi_{\max}$. □

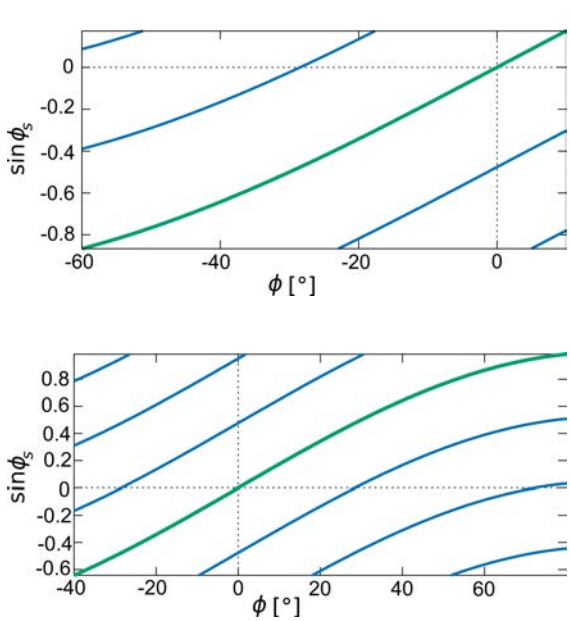

Fig. 30. The diagrams of shifted sine curves for different ranges of angles ϕ and their corresponding ranges of sine values: a) $\Phi = [-60°, 10°]$, b) $\Phi = [-40°, 80°]$.

The feature proved in Theorem 1 makes it possible to obtain a simple geometrical interpretation of a procedure of $D^{\sin}_{\Phi}$ determination for given b_{01} and b_{12}. Considering the case of $\phi_{\min}$, to compute $D^{\sin}_{\Phi}(b_{01}, b_{12})$ it means finding the minimal distance between the points of two sequences in the range of $[\sin\phi_{\min}, \sin\phi_{\max}]$, whose common origin is the value $\sin\phi_{\min}$ (see Fig. 31). The points of each of these sequences are equally spaced by distances $\frac{\lambda}{b_{01}}$ and $\frac{\lambda}{b_{12}}$, respectively.

Set $\mathcal{I}_{\Phi}(.)$ creates an interval of integer numbers. Using (4), it is useful to define the size of the interval of e.g. $\mathcal{I}_{\Phi}(\phi, b)_{\phi}$ as follows

$$\Delta^{\mathcal{I}}_{\Phi}(b) = \left\lfloor \frac{b(\sin\phi_{\max} - \sin\phi_{\min})}{\lambda} \right\rfloor.$$

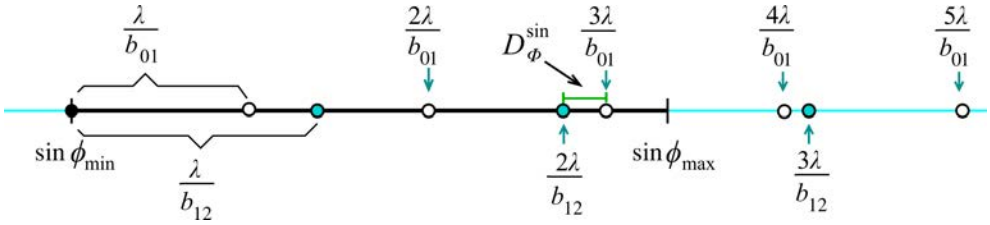

Fig. 31. Two sequences of solution values of Eq. (3), which are generated by receiver pairs (R_0, R_1) and (R_1, R_2) for the azimuth angle $\phi = \phi_{\min}$.

Theorem 2. Considering the ultrasonic system presented in Fig. 7, in which the sensitivity ranges of all receivers are $\Phi = [\phi_{\min}, \phi_{\max}] \subset \left(-\frac{\pi}{2}, \frac{\pi}{2}\right)$, if $D_{\Phi}^{\sin}(b_{01}, b_{12}) = 0$ then integer numbers k_i and k_j exist such that

$$0 < k_i \le \Delta_{\Phi}^{\mathcal{I}}(b_{01}) \ \wedge \ 0 < k_j \le \Delta_{\Phi}^{\mathcal{I}}(b_{12})$$

and

$$k_j b_{01} = k_i b_{12}.$$

Proof: If $D_{\Phi}(b_{01}, b_{12}) = 0$ then taking into account Theorem 1, it means that

$$\exists \phi' \in \Phi; \quad \phi' \neq \phi_{\max} \wedge \phi' \in \mathcal{A}_{\Phi}(\phi_{\max}, b_{01})_{\phi} \cap \mathcal{A}_{\Phi}(\phi_{\max}, b_{12})_{\phi}. \tag{25}$$

Because of (5), there are integer numbers $n_i \in \mathcal{I}_{\Phi}(\phi_{\max}, b_{01})_{\phi}$ and $n_j \in \mathcal{I}_{\Phi}(\phi_{\max}, b_{12})_{\phi}$ such that

$$\sin\phi_{\max} = \frac{v_a\tau_{01}(\phi_{\max}) + n_i\lambda}{b_{01}} = \frac{v_a\tau_{12}(\phi_{\max}) + n_j\lambda}{b_{12}}. \tag{26}$$

Because of (25) there exist integer numbers $n_i' \in \mathcal{I}_{\Phi}(\phi_{\max}, b_{01})_{\phi}$ and $n_j' \in \mathcal{I}_{\Phi}(\phi_{ax}, b_{12})_{\phi}$ such that

$$\sin\phi' = \frac{v_a\tau_{01}(\phi_{\max}) + n_i'\lambda}{b_{01}} = \frac{v_a\tau_{12}(\phi_{\max}) + n_j'\lambda}{b_{12}}. \tag{27}$$

The numbers n_i' and n_j' can be expressed by n_i and n_j as follows

$$n_i' = n_i + k_i, \qquad n_j' = n_j + k_j. \tag{28}$$

Because

$$n_i, n_i' \in \mathcal{I}_{\Phi}(\phi_{\max}, b_{01})_{\phi}$$

and because $k_i = n_i' - n_i$ and $n_i' \neq n_i$, thus

$$0 < |k_i| \le \Delta_{\Phi}^{\mathcal{I}}(b_{01}). \tag{29}$$

A similar line of reasoning can be applied to k_j, which gives the conclusion

$$0 < |k_j| \le \Delta_{\Phi}^{\mathcal{I}}(b_{12}).$$

Substituting (28) to (27), the following is obtained

$$\frac{v_a\tau_{01}(\phi_{\max}) + n_i\lambda + k_i\lambda}{b_{01}} = \frac{v_a\tau_{12}(\phi_{\max}) + n_j\lambda + k_j\lambda}{b_{12}}. \tag{30}$$

Using (26), the equation is reduced to the form

$$\frac{k_i}{b_{01}} = \frac{k_j}{b_{12}}. \tag{31}$$

Knowing that $b_{01}, b_{12} > 0$, k_i and k_j have to be simultaneously negative or positive values. For both cases, the same values of b_{01} and b_{12} are obtained. Thus, it is enough to consider only positive values. It allows the condition (29) to be rewritten into the form

$$0 < k_i \le \Delta_{\Phi}^{\mathcal{I}}(b_{01}).$$

The same can be said about k_j. □

To exemplify the described feature, the diagram presented in Fig. 10 can be considered. Analysing its border created for the case $b_{01} = 30$ and $10 \le b_{12} \le 30$, it can be noticed that $D_{\Phi}^{\sin}$ is 0 when $b_{12} = 10$, 12, 15, 18, 20, 22.5, 24, 25, 30 mm. To have a better view, this section of the diagram is presented in Fig. 32. The respective values of (k_j, k_i) are $(1,3)$, $(2,5)$, $(1,2)$, $(3,5)$, $(2,3)$, $(3,4)$, $(4,5)$, $(5,6)$, $(1,1)$.

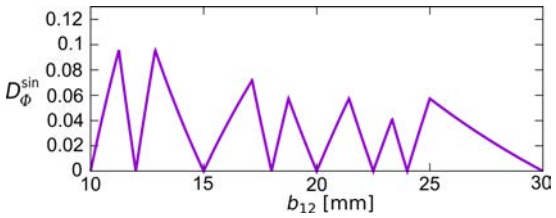

Fig. 32. The dependence of $D_{\Phi}^{\sin}$ on the values of b_{12} when $b_{01} = 30$ mm.

Theorem 3. Considering the ultrasonic system presented in Fig. 7, in which the sensitivity ranges of all receivers are $\Phi = [\phi_{\min}, \phi_{\max}] \subset \left(-\frac{\pi}{2}, \frac{\pi}{2}\right)$, when relatively prime positive integer numbers k_p and k_q exist such that $k_p \neq k_q$ and

$$\sin\phi_{\max} - \sin\phi_{\min} = \frac{k_p\lambda}{b_{01}} = \frac{k_q\lambda}{b_{12}} \tag{32}$$

then $D_{\Phi}^{\sin}$ is discontinuous at the points (b_{01}, b_{12}) and (b_{12}, b_{01}).

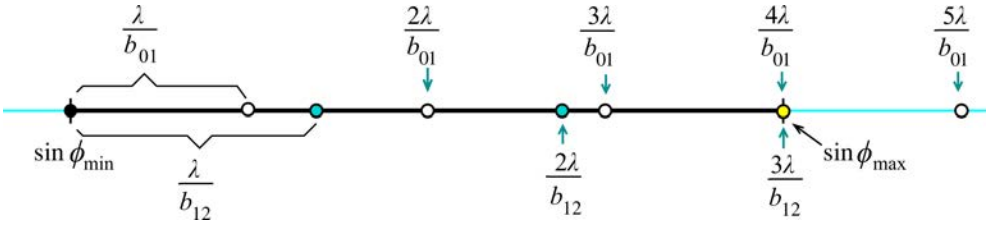

Fig. 33. Two sequences of the solution values of Eq. (3) generated by receiver pairs (R_0, R_1) and (R_1, R_2) for the azimuth angle $\phi_{\min}$ with a common point at the right border of the range of $[\sin\phi_{\min}, \sin\phi_{\max}]$.

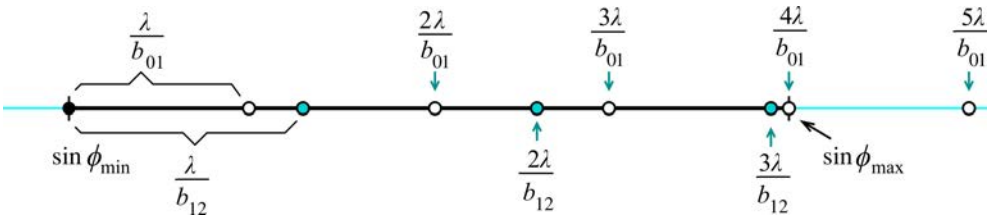

Fig. 34. Two sequences of the solution values of Eq. (3) generated by receiver pairs (R_0, R_1) and (R_1, R_2) for the azimuth angle $\phi_{\min}$.

Proof: Since

$$\Delta^{\mathcal{I}}_{\Phi}(b_{01}) = k_p \ \wedge \ \Delta^{\mathcal{I}}_{\Phi}(b_{12}) = k_q,$$

and because of Theorem 2,

$$D^{\sin}_{\Phi}(b_{01}, b_{12}) = 0.$$

Using the geometrical interpretation presented in Fig. 31, Eq. (3) means that the points of both sequences referring to b_{01} and b_{12} and generated for $\phi^{\star}$ meet each other at the border of the range $[\sin\phi_{\min}, \sin\phi_{\max}]$. Such a situation is illustrated in Fig. 33. Because numbers k_p and k_q are relatively prime, such a case cannot happen inside the range $[\sin\phi_{\min}, \sin\phi_{\max}]$. It is obvious that k_p and k_q must be bigger than 1, and because the sequences of numbers are finite, there exists $\delta > 0$ that

$$\delta < \min_{k_i \in [1, k_p - 1]_{\mathbf{I}} \wedge k_j \in [1, k_q]_{\mathbf{I}}} \left| \frac{k_i \lambda}{b_{01}} - \frac{k_j \lambda}{b_{12}} \right|.$$

It is possible to choose $\varepsilon > 0$ so that, for all $\varepsilon' \in (0, \varepsilon]$ and $b'_{01} = b_{01} - \varepsilon'$ the following condition is met

$$\delta < \min_{k_i \in [1, k_p - 1]_{\mathbf{I}} \wedge k_j \in [1, k_q]_{\mathbf{I}}} \left| \frac{k_i \lambda}{b'_{01}} - \frac{k_j \lambda}{b_{12}} \right|.$$

When $\varepsilon < \frac{b_{01}}{k_p}$, then

$$\Delta^{\mathcal{I}}_{\Phi}(b'_{01}) = k_p - 1.$$

Therefore

$$D^{\sin}_{\Phi}(b'_{01}, b_{12}) = \min_{k_i \in [1, k_p - 1]_{\mathbf{I}} \wedge k_j \in [1, k_q]_{\mathbf{I}}} \left| \frac{k_i \lambda}{b'_{01}} - \frac{k_j \lambda}{b_{12}} \right|.$$

It means that

$$D^{\sin}_{\Phi}(b_{01}, b_{12}) = 0 \quad \wedge \quad \forall b'_{01} \in [b_{01} - \varepsilon, b_{01}); \quad D^{\sin}_{\Phi}(b'_{01}, b_{12}) > \delta.$$

□

The discontinuities of $D^{\sin}_{\Phi}$ observed in Figs 10 and 11 have a characteristic shape of corners. The biggest *jump* is at the vertex of a corner, and it is then reduced along each edge. To explain this, the example presented in Fig. 34 can be considered. In this example, it is simple to notice that

$$\exists \delta > 0; \quad D^{\sin}_{[\phi_{\min},\, \phi_{\max})}(b_{01}, b_{12}) - D^{\sin}_{[\phi_{\min},\, \phi_{\max}]}(b_{01}, b_{12}) > \delta.$$

Then, when b_{01} is slightly decreased, the last point is outside of $[\sin\phi_{\min}, \sin\phi_{\max}]$. Therefore

$$\exists \varepsilon' > 0, \quad \forall \varepsilon \in (0, \varepsilon']; \quad D^{\sin}_{[\phi_{\min},\, \phi_{\max}]}(b_{01} - \varepsilon, b_{12}) - D^{\sin}_{[\phi_{\min},\, \phi_{\max}]}(b_{01}, b_{12}) > \delta.$$

This discontinuity is observed for values of b_{12} which belongs to the range $[b'_{12}, b''_{12})$ in which the distance between points determined by $\frac{3\lambda}{b_{12}}$ and $\frac{4\lambda}{b_{01}}$ is the smallest (see Fig. 34). The left boundary of the range determines the beginning point (b_{01}, b'_{12}) of the bifurcation at which

$$D^{\sin}_{[\phi_{\min}, \phi_{\max}]}(b_{01}, b'_{12}) = 0.$$

In the example presented in Fig. 34, it is when $\frac{3\lambda}{b'_{12}} = \frac{4\lambda}{b_{01}}$. The right boundary of the range determines the point (b_{01}, b''_{12}) at which the discontinuity disappears i.e.

$$D^{\sin}_{[\phi_{\min}, \phi_{\max})}(b_{01}, b''_{12}) - D^{\sin}_{[\phi_{\min}, \phi_{\max}]}(b_{01}, b''_{12}) = 0.$$

By changing places of b_{01} and b_{12} in Fig. 34, the same can be said about b_{01}. It means that the discontinuity extends along two perpendicular lines which start at the same vertex.

References

1. Choi K.H., Ra W., Park S., Park J.B. (2014), *Robust least squares approach to passive target localization using ultrasonic receiver array*, IEEE Transactions on Industrial Electronics, **61**, 4, 1993–2002, doi: 10.1109/TIE.2013.2266076.
2. Clapp M.A., Etienne-Cummings R. (2006), *Single Ping-multiple measurements: sonar bearing angle estimation using spatiotemporal frequency filters*, Circuits and Systems I: Regular Papers, IEEE Transactions on, **53**, 4, 769–783, doi: 10.1109/TCSI.2005.859613.
3. Haardt M., Nossek J.A. (1995), *Unitary ESPRIT: how to obtain increased estimation accuracy with a reduced computational burden*, IEEE Transactions on Signal Processing, **43**, 5, 1232–1242, doi: 10.1109/78.382406.
4. Herman K., Gudra T., Furmankiewicz J. (2014), Digital signal processing approach in air coupled ultrasound time domain beamforming, Archives of Acoustics, 39, 1, 27–50, doi: 10.2478/aoa-2014-0005, url: http://acoustics.ippt.gov.pl/index.php/aa/article/view/1480.
5. Im A. *et al.* (2013), *DOA Estimation via Phase Measurement*, [in:] Progress in Electromagnetics Research Symposium, Taipei, Taiwan.
6. Kabała M., Wnuk M. (2005), *Module with microcontroller MC9S12A64* [in Polish: *Moduł z mikrokontrolerem MC9S12A64*], Tech. rep. SPR nr 11/2005, Institute of Computer Science, Automatics and Robotics of the Wroclaw University of Technology.
7. Kleeman L., Kuc R. (1995), *Mobile robot sonar for target localization and classification*, International Journal of Robotics Research, **14**, 4, 295–318.
8. Kreczmer B. (2017), *Azimuth angle determination for the arrival direction for an ultrasonic echo signal*, Journal of Automation, Mobile Robotics and Intelligent Systems, **11**, 02, 31–41. doi: 10.14313/JAMRIS_2-2017/14.
9. Kreczmer B. (2018), *Azimuth angle estimation of ultrasonic signal arrival by using multi-pair receiver system*, [in:] *"Automation 2018", Advances in Intelligent Systems and Computing*, Springer International Publishing, pp. 672–681.
10. Roy R., Kailath T. (1989), *ESPRIT – estimation of signal parameters via rotational invariance techniques*, IEEE Transactions on Acoustics, Speech, and Signal Processing, **37**, 7, 984–995, doi: 10.1109/29.32276.
11. Roy R., Paulraj A., Kailath T. (1986), *Direction-of-arrival estimation by subspace rotation methods – ESPRIT'*, [in:] ICASSP '86. IEEE International Conference on Acoustics, Speech, and Signal Processing, vol. 11, pp. 2495–2498, doi: 10.1109/ICASSP.1986.1168673.
12. Schmidt R. (1986), *Multiple emitter location and signal parameter estimation*, IEEE Transactions on Antennas and Propagation, **34**, 3, 276–280, doi: 10.1109/TAP.1986.1143830.
13. Steckel J., Boen A., Peremans H. (2013), *Broadband 3-D Sonar system using a sparse array for indoor navigation*, IEEE Transactions on Robotics, **29**, 1, 161–171, doi: 10.1109/TRO.2012.2221313.
14. Steckel J., Peremans H. (2013), *BatSLAM: Simultaneous localization and mapping using biomimetic sonar*, PLOS ONE, **8**, 1, 1–11, doi: 10.1371/journal.pone.0054076, url: https://doi.org/10.1371/journal.pone.0054076.
15. Steckel, J., Peremans H. (2015), *Spatial sampling strategy for a 3D sonar sensor supporting BatSLAM*, [in:] 2015 IEEE/RSJ International Conference on Intelligent Robots and Systems (IROS), pp. 723–728, doi: 10.1109/IROS.2015.7353452.
16. Sun F., Lan P., Gao B. (2015), *Partial spectral search-based DOA estimation method for co-prime linear arrays*, Electronics Letters, **51**, 24, 2053–2055, doi: 10.1049/el.2015.2261.
17. Tayem N., Kwon H.M. (2003), *Conjugate ESPRIT (C-SPRIT)*, [in:] IEEE Military Communications Conference, MILCOM 2003, Vol. 2, pp. 1155–1160, doi: 10.1109/MILCOM.2003.1290358.
18. Walter C., Schweinzer H. (2014), *Locating of objects with discontinuities, boundaries and intersections using a compact ultrasonic 3D sensor*, [in:] 2014 International Conference on Indoor Positioning and Indoor Navigation, pp. 99–102.
19. Yang X. *et al.* (2018), A fast and robust DOA estimation method based on JSVD for co-prime array, IEEE Access, **6**, 41697–41705, doi: 10.1109/ACCESS.2018.2860680.
20. Zhang D., Zhang Y., Zheng G., Feng C., Tang J. (2017), *Improved DOA estimation algorithm for co-prime linear arrays using root-MUSIC algorithm*, Electronics Letters, **53**, 18, 1277–1279, doi: 10.1049/el.2017.2292.
21. Zhou C., Shi Z., Gu Y., Shen X. (2013), *DECOM: DOA estimation with combined MUSIC for coprime array*, [in:] 2013 International Conference on Wireless Communications and Signal Processing, pp. 1–5, doi: 10.1109/WCSP.2013.6677080.